



ELSEVIER

Contents lists available at ScienceDirect

## International Journal of Adhesion and Adhesives

journal homepage: [www.elsevier.com/locate/ijadhadh](http://www.elsevier.com/locate/ijadhadh)

## Characterizing fracture performance and the interaction of propagating cracks with locally weakened interfaces in adhesive joints

Shantanu R. Ranade<sup>a</sup>, Youliang Guan<sup>b</sup>, Robert B. Moore<sup>c</sup>, John G. Dillard<sup>c</sup>, Romesh C. Batra<sup>b</sup>, David A. Dillard<sup>b,\*</sup>

<sup>a</sup> Macromolecular Science and Engineering, Virginia Polytechnic Institute and State University, Blacksburg, VA 24061, United States

<sup>b</sup> Biomedical Engineering and Mechanics Department, Virginia Polytechnic Institute and State University, Blacksburg, VA 24061, United States

<sup>c</sup> Department of Chemistry, Virginia Polytechnic Institute and State University, Blacksburg, VA 24061, United States

### ARTICLE INFO

#### Keywords:

Fracture energy  
Tailored interfaces  
Crack path selection  
Falling or reverse R-curve  
Double cantilever beam (DCB) tests

### ABSTRACT

This paper experimentally investigates adhesive fracture resistance and crack path selection in adhesive joints containing well-defined localized interfacial defects. Several systematic patterns of localized interfacial defects were created on base-acid treated aluminum adherends by physical vapor deposition of copper through a mask. Adhesive joints were prepared using a commercially available, structural epoxy adhesive and the effect of localized interface defects on the performance of adhesive joints was studied. Under mode-I loading conditions, the presence of localized weak interfaces influenced the fracture energy of a propagating debond over a considerable distance. For a crack tip approaching a given weak interface pattern, a falling or reverse R-curve type trend was observed. Within the same DCB specimen, as the crack tip advanced beyond the patterned region, a rising R-curve type trend was observed as fracture energy increased with increasing crack lengths, which were recorded visually and were also inferred using compliance and crack length relationship. In addition, the mode-I fracture energy was found to scale with the area fraction of the weak interfaces according to a rule of mixtures. For the adhesive system and the joint geometry used in this study, it was observed that cohesive failure in the adhesive layer can be obtained even in the presence of exceptionally weak interfaces (similar in size to those detected in mode-I loading) when loaded under mixed mode conditions (achieved through asymmetric loading of DCB-like specimens), that tended to steer the crack away from the interface. When loaded with the opposite mode mixity direction, the crack tip propagated through the defects, though the fracture energy did not exhibit similar R-curve type trends as observed in mode-I tests. The results offer insights into the interaction of propagating cracks in adhesive layers and their interactions with discrete, localized defects, which could lead to improvements in surface preparations and bond integrity or even to joint designs having intentionally placed defects useful in controlled disassembly or for other purposes.

### 1. Introduction

Identifying the locus of failure in adhesive joints is important for understanding and interpreting bond performance. The crack path selection process, which determines the resulting locus of failure and the associated fracture resistance in adhesive bonds, involves a complex interaction of the spatially varying stress state ahead of a growing crack tip with the material system's resistance to failure, as demonstrated theoretically [1] and experimentally, including as affected by thermally [2] and mechanically induced [3] residual stresses, and with the presence of a supporting scrim layer [4]. Though a number of studies have been carried out to understand effects of joint geometry [5,6], fracture mode mixity [7], and material properties [8] on crack path selection

and the performance of adhesive bonds, several studies have probed crack path selection and adhesive joint fracture performance in the presence of localized interfacial defects. Examples include peeling of tapes from a patterned ink layer on a silicone substrate [9], fracture of micro-patterned roughness domains for microelectronic encapsulant adhesion [10] and patterned silane treatments on aluminum (oxide) surfaces as measured with climbing drum tests [11]. Budzik et al. reported that weak interfaces reduce the overall adhesion more than that would be expected from a linear reduction in bond area [12]. Chopin et al. studied the spatiotemporal dynamics of a crack front propagating at the interface for patterned substrate with a single defect [13]. Cuminatto et al. proposed an analytical model to characterize the debonding of patterned substrates, highlighting the role of pattern

\* Correspondence to: BEAM Dept (0219), Virginia Tech, Blacksburg, VA 24061, United States.  
E-mail address: [dillard@vt.edu](mailto:dillard@vt.edu) (D.A. Dillard).

periodicity and line width on interfacial mechanical behavior during debonding [14]. Dalmas et al. studied the effect of macroscopic unidimensional patterns in the direction of crack propagation on crack front morphology [15]. Tvergaard et al. studied the role of micron scale patterning on the interface toughness using patterned wafer level Cu-Cu bonds wherein 400 nm Cu films were deposited in a variety of patterns on Si wafer substrates [16]. Reedy conducted a finite element analysis to determine interfacial toughness dependence of brittle, thin film material systems on nano-scale interfacial roughness using parallel rectangular-toothed or rippled cross-section shaped patterns [17].

During the manufacture of adhesive joints, it is difficult to completely prevent defects in adhesive joints. These defects can be in the form of voids, improperly mixed or cured adhesive in some locations, adherend surface contaminations, etc. The presence of such defects can lead to weakened interfaces with reduced stiffness or load carrying capabilities or disbonds that are incapable of resisting certain tractions at the interface of an adhesive joint. In adhesive joints, disbonds with traction-free surfaces can often be detected using non-destructive techniques, however, it is difficult to detect weakened interfaces that retain partial integrity [18].

An improved understanding of fracture resistance and crack path selection in the presence of localized interfacial defects might lead to adhesive joints with tunable failure locus and resistance to fracture. Such joints might be useful in applications that require controlled disassembly of adhesive joints, such as the packaging industry, and perhaps other fields where recycling and reuse options offer enhanced sustainability. This paper experimentally investigates adhesive fracture performance and crack path selection in epoxy-bonded double cantilever beam (DCB) specimens containing well-defined and quantifiable localized interfacial defects created using a physical vapor deposition technique to deposit copper on aluminum adherends.

## 2. Experimental

### 2.1. DCB tests

All DCB specimens were prepared using 6061-T6511 aluminum bars as adherends, having dimensions of 305 mm × 25.4 mm × 12.7 mm. Holes were drilled at the midplane on one end of each aluminum bar to accommodate loading pins. The bonding surfaces of the adherends were then abraded with #220 sandpaper. Abraded adherends were washed with deionized (DI) water and treated with a sodium hydroxide (base) solution and rinsed again with DI water. The adherends were then immersed in a nitric acid solution and rinsed with DI water again before being dried for 2 h at 120 °C. This procedure is typically referred to as “base-acid treatment” and details of which are reported in [8]. The joints consisted of two such control adherends, but for most specimens, one of the adherends was subsequently modified to form locally weakened regions on the bonding surface. Several patterns of local weak interfaces were created on base-acid treated aluminum adherend surfaces utilizing physical vapor deposition (PVD) of copper (99.99% pure) with a Kurt-Lesker PVD-250 instrument. Acrylic masks (1.27 mm thickness) with desired patterns were prepared using an Epilog laser cutter (64 W). The acrylic masks were cleaned with compressed nitrogen gas and acetone prior to use, then mounted on the adherends to be treated. The acrylic mask was placed on the adherend such that it covered the entire area of the bonding surface except for the patterns on the masks. Physical vapor depositions were carried out at 25 °C in a clean room environment at  $6.6 \times 10^{-4}$  Pa pressure and at a deposition rate of about 0.25 nm/s. The final thickness of the deposited copper film was about 250 nm. Fig. 1 summarizes the procedure used to create libraries of patterns containing localized weak interfaces for a given specimen. As discussed in a later section, each copper deposited region within a pattern forms a local weak interface due to poor adhesion between the deposited copper and the aluminum adherends.

Fig. 2 summarizes dimensions of the weak interface patterns for all

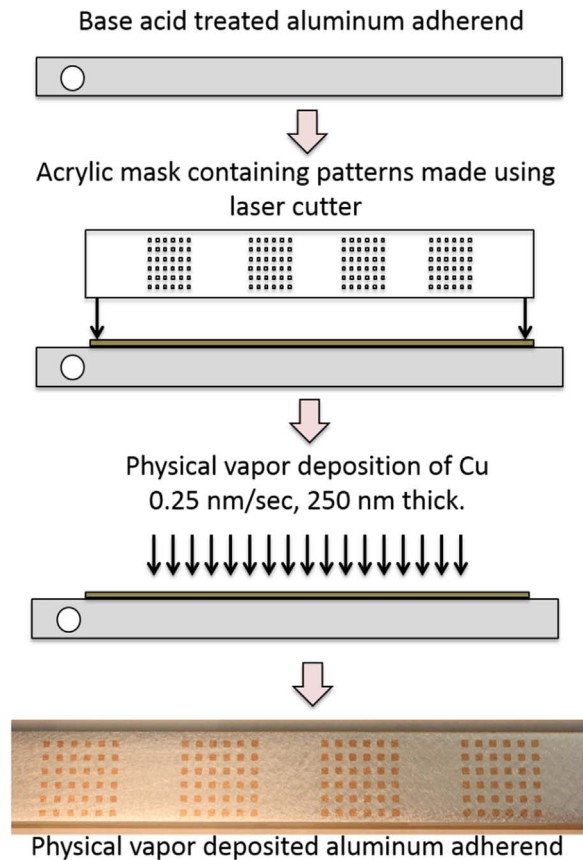


Fig. 1. Procedure used to create patterns with locally weak interfaces on the bonding surface of base-acid treated aluminum adherends.

tested specimens and the crack grew from left to right in subsequent DCB testing. The left edge of each schematic diagram represents the position of loading holes with respect to the first pattern. Except for specimens of type B (two replicates), one specimen was tested from each other specimen type. A detailed discussion on the choice of a particular pattern is included in Section 3.

A commercially available toughened structural epoxy adhesive (LORD™ 320/322) was used to bond the prepared aluminum adherends. For all specimens, a bondline thickness of 0.2 mm was maintained by placing spacers at each end of the specimen during assembly. Per the adhesive manufacturer's recommendation, specimens were cured for 14 h at room temperature and post-cured at 60 °C for 3 h. All DCB tests (mode-I and mixed mode) were carried out at a net crosshead rate of 0.1 mm/min. A 5800R Instron tensile testing machine was used for mode-I tests while mixed mode tests were carried out using a dual actuator load frame and using a global mode mixity angle ( $\psi$ ) of 60° in all mixed mode tests. Details of dual actuator load frame and mode mixity calculations are described in [19]. Mode-I and mixed mode fracture energies were calculated using corrected beam theory as described in the ISO-25217:2009 standard,

$$\mathcal{G}_{Ic} = \frac{3P\delta}{2B(a + \hat{a})}F \quad (1)$$

where  $\mathcal{G}_{Ic}$  is mode-I fracture energy,  $P$  is the load measured by the load cell,  $a$  is the crack length,  $\delta$  is the crosshead displacement at crack length  $a$ ,  $F$  is the large displacement correction,  $B$  is the width of the specimen and of the bond, and  $\hat{a}$  is the crack length correction.

During the DCB tests, crack lengths were measured by visual observation of the crack tip using a magnifying glass. This limits the number of data points that can be gathered for a given specimen. For a DCB specimen with drilled holes, the flexural modulus ( $E_f$ ) relates with

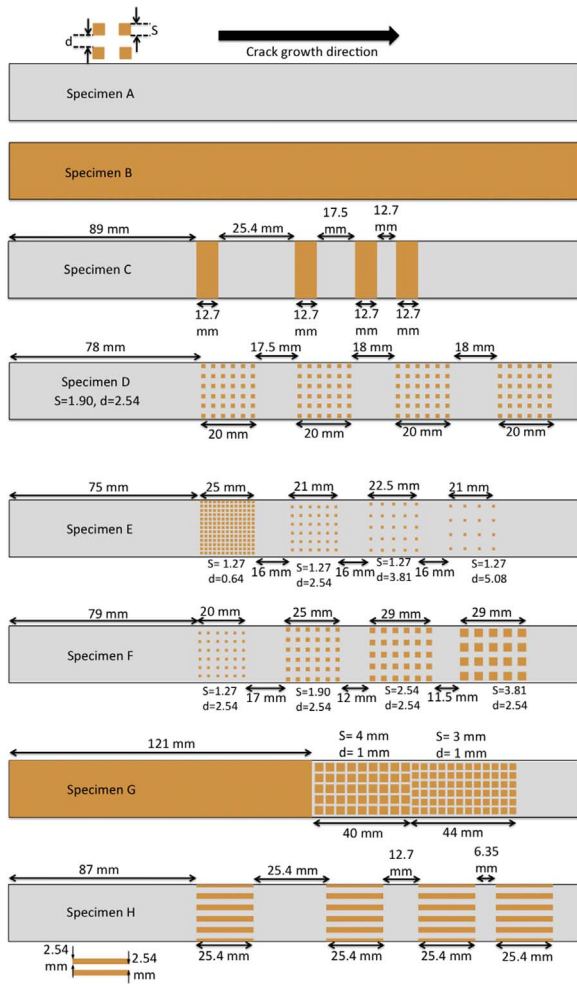


Fig. 2. Schematic representation and dimensions of weak interface topology in specimens used in the study.

the compliance of the specimen and the measured crack length as (ISO-25217:2009 standard)

$$E_f = \frac{8(a + \hat{a})^3}{CBh^3} \quad (2)$$

$$\text{where, } C = \frac{\delta}{P}$$

Rearranging Eq. (2) leads to,

$$C = \left[ \frac{8}{E_f Bh^3} \right] (a + \hat{a})^3 \quad (3)$$

Since load and beam deflections (crosshead displacements) were measured automatically every 0.1 s during the tests, from which compliance could be determined, the compliance as a function of visually observed crack length could be fit using Eq. (3) (typically with  $R^2 > 0.999$ ), from which one could infer crack lengths over an entire test. These inferred values are referred to as estimated fracture energies in subsequent figures; their use permitted a more complete understanding of the evolving fracture resistance. Using Eq. (1), fracture energies were then calculated from visually observed crack lengths as well as from inferred crack lengths.

## 2.2. Single edge notch bend (SENB) tests

SENB tests were used to calculate the plane stress fracture toughness ( $K_{Ic}$ ) of the bulk adhesive, following the ASTM D 5045-99 standard.

Epoxy specimens were cast using silicone molds and cured at the same conditions reported above for the DCB test specimens. The SENB specimens had dimensions of about 57.1 mm × 12.7 mm × 6.3 mm (length × width × thickness). Specimens were pre-cracked by driving a fresh, sharp razor blade with gentle tapping such that the crack tip was a few millimeters ahead of the razor blade tip. Crack lengths were measured using high-resolution images of the pre-cracked specimens and digital image analysis software (Photron FASTCAM Analysis, Photron USA Inc., San Diego, CA, USA). Pre-cracked specimens were then mounted crack down on a 3-point bend fixture in a 5500R Instron and loaded at a constant crosshead rate of 0.1 mm/min to failure. Plane stress fracture toughness values were calculated per ASTM D 5045-99 standard utilizing tensile yield strength ( $\sigma_{y \text{ tensile}}$ ) values estimated from compression tests as described in the next section. The plane stress plastic zone size,  $r_p$ , was estimated using the following expression.

$$\text{Plane stress plastic zone size} = \frac{1}{2\pi} \left( \frac{K_{Ic}}{\sigma_{y \text{ tensile}}} \right)^2 \quad (4)$$

where  $K_{Ic}$  is the plane strain fracture toughness.

## 2.3. Compression tests on the bulk adhesive

Dogbone specimens tested in tension to obtain tensile yield strength values failed in a brittle manner before yielding, precluding the use of tensile tests for obtaining the tensile yield strength values. For a toughened epoxy system, it has been reported that the tensile yield strength is approximately 75% of the compressive yield strength [20]. For compression tests, three cylindrical specimens were cast and then machined to a height/diameter ratio between 1.5 and 2.0 (ASTM-D695-10 standard). The specimens were loaded between polished steel platens in an Instron 5500R test frame at a crosshead rate of 0.1 mm/min. The compressive yield strength ( $\sigma_{y \text{ compression}}$ ) was determined by applying a 1% strain offset to the resulting compressive stress vs. strain curves.

## 3. Results and discussion

### 3.1. Mode-I test results

Specimens of type A and B were control specimens having uniform surface treatments. Fig. 3 shows representative failure modes and a schematic representation of the observed failure locus for type A specimens (base-acid treated adherends) and type B specimens (100% PVD copper coating on one adherend bonding surface). Visual examinations of the failure surfaces revealed cohesive failure within the adhesive layer for type A specimens and apparent interfacial failure at the copper/aluminum interface for type B specimens. Repeatability of the observed failure modes was confirmed by testing four DCB specimens of type B and two specimens of type A, with representative mode-I DCB fracture energy results shown in Fig. 4. For type B specimens, the crack propagated at relatively high speeds through the copper/aluminum interface, thus very few data points could be gathered. The collected data suggested interfacial fracture energy of about 20 J/m<sup>2</sup> (calculated using Eq. (1)). These fracture energies were much lower than the average fracture energy (for multiple points on the same specimens) of about 460 J/m<sup>2</sup> obtained for cohesive failures in type A specimens. When coupled with exposure masks, these results suggest that the PVD technique could enable the preparation of locally weakened interfaces having an interfacial fracture energy approximately 4.5% of the fracture energy of an adhesive joint having good interfaces that resulted in cohesive failures.

As shown schematically in Fig. 2, specimen C had four localized weak interfaces, separated by control regions, covering the entire width of the specimen. When tested in mode-I, the specimen C pattern should offer insights into the performance of an adhesive joint in which a propagating crack is approaching a localized weak interface of

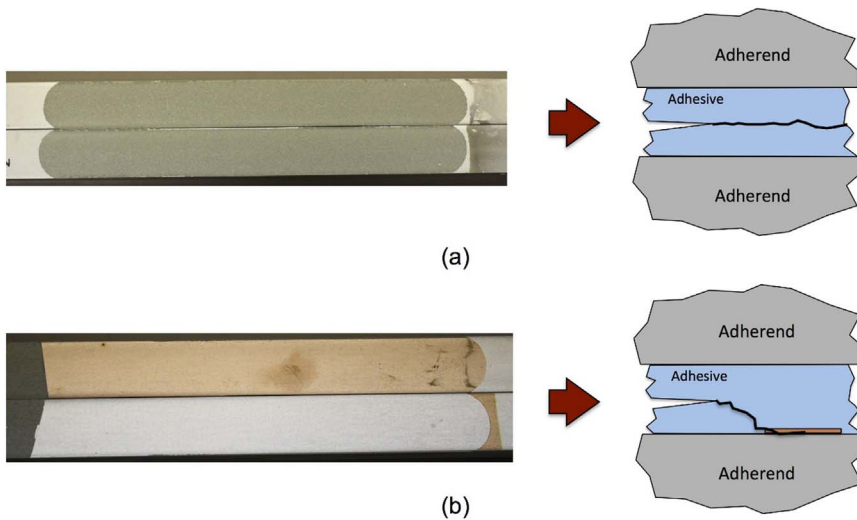


Fig. 3. Failure surfaces for mode-I DCB tests (a) cohesive failure within adhesive layer for type A specimen (control specimen), (b) apparent interfacial failure at copper/aluminum interface for a DCB specimen with PVD copper coating on the entire surface of one adherend (specimen type B).

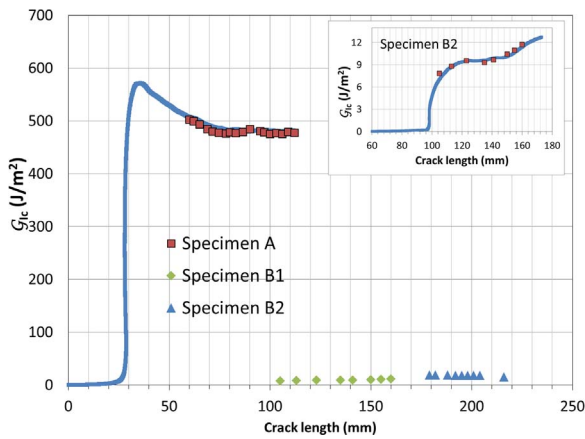


Fig. 4. Mode-I DCB test results for control specimens, a representative specimen type A with no copper coating on either adherend and for type B specimens with one adherend having a PVD copper coating over the entire bonding surface. Red squares denote experimentally observed crack lengths and blue squares represent estimated crack lengths inferred from load and displacement results. The inset shows expanded view of the data from specimen B2. (For interpretation of the references to color in this figure legend, the reader is referred to the web version of this article.)



Fig. 5. Failure surfaces of specimen C, suggesting interfacial failures in copper covered regions.

significant width. Also, the control region length between successive localized weak interfaces decreased progressively, allowing us to probe the effect of separation distance between weakened interfaces on the fracture performance of the adhesive in the control regions. Fig. 5 shows failure surfaces of specimen C when tested under mode-I conditions. Similar to failure modes shown schematically in Fig. 3, the copper deposited regions in specimen C showed an apparent interfacial failure at the copper/adherend interface, while regions without copper depositions (control regions) resulted in cohesive failures. Fig. 6 shows mode-I fracture results for specimen C with localized weak interface regions highlighted in light copper red color (Here, the crack length is based on the visually observed crack tip at the edge of the specimen,

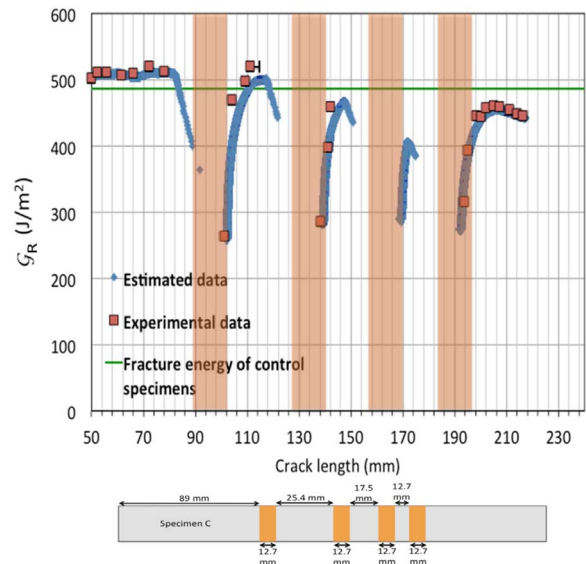


Fig. 6. Mode-I DCB test results and schematic representation of the weak interface patterns (orange in color) for specimen C, where shaded bars denote nominal locations of weakened zones, red squares denote experimentally observed crack lengths and blue diamonds represent estimated crack lengths inferred from load and displacement results. (For interpretation of the references to color in this figure legend, the reader is referred to the web version of this article.)

though the actual crack length varied somewhat across the width of the specimen).

To interpret the fracture response, recall that rising crack resistance or R-curve behavior, results from the growing size of the plastic or damage zone following crack initiation. Rising R-curve behavior has been reported in adhesive joints by Papini et al. [21], though the unambiguous identification of crack propagation required for R-curve construction complicates determination. Crack propagation in toughened structural adhesive joints is believed to begin with energy dissipation mechanisms such as cavitation, micro-cracking, and shear banding, these mechanisms lead to growth of a cohesive zone that consists of yielded material and distributed micro-cracks [22]. With further loading of the specimen, the micro-cracks coalesce and form a macro-crack, which then propagates with formation of new micro-cracks and the plastic zone into the adhesive layer [23]. Thus during initial stages of fracture, the plastic zone may continue to expand, leading to a progressive toughening of the joint as input energy is dissipated by the plastic deformation. Depending on how one defines

the crack length, this process can result in a rising fracture resistance curve (R-curve) that eventually plateaus when the cohesive zone reaches a steady-state size and the fracture resistance becomes constant.

Returning to Fig. 6, rising R-curve-like trends are observed as the propagating crack approached each of the control regions. In Fig. 6 and in the following sections, fracture energy data based on experimentally measured crack lengths is shown using red squares (captioned as “Experimental data”), while the fracture energies calculated using estimated crack lengths (Eq. (3)) are shown using small blue diamond data markers (captioned as “Estimated data”). In the long initial control region (crack length of 50–90 mm), the resistance curve plateau value is similar to that measured for control type A specimens. The fracture energy of the adhesive joint was not affected until the visually observed crack tip was within about 8 to 10 mm from the first localized weak interface. In the next control region (100–127 mm), a rising R-curve and a possible plateau is observed. This process is repeated in each subsequent control zone, with drops in fracture resistance initiating similar distances ahead of each weak zone (except near the end of the specimen). The shorter subsequent control regions are insufficient for R-curve plateau development, resulting in successively smaller values of the peak resistance with shorter control lengths.

Studies have shown that for a thin bondline thickness DCB specimens, where height of the plane stress plastic zone is of the order of or greater than the bondline thickness of the specimens, local tensile stresses ahead of the crack tip remain high over a considerably longer distance than that with bulk adhesive specimens [20]. Based on such studies, it has been suggested that for thin bondline DCB specimens bonded with a toughened structural epoxy adhesive, the plastic zone ahead of the crack tip can be considerably longer in length compared to the plastic zone length in bulk adhesive specimens [20,24]. The plane stress plastic zone height in a bulk adhesive specimen can be estimated using Eq. (4). Table 1 lists the average plane stress fracture toughness obtained from the SENB tests, results from compression tests, and the average plane stress plastic zone diameter or height calculated by doubling the result from Eq. (4).

From SENB tests, the plane stress plastic zone height for bulk adhesive specimens was around 0.17 mm, which is very similar to the bondline thickness (0.2 mm) used in this study. Thus the onset of reverse R-curve trends at 8 to 10 mm prior to weak interfaces might be due to longer plastic zone that develops ahead of the crack tip. In light of a longer plastic zone, the reverse R-curve type trends might be due to plastic zone dimensions ahead of the crack tip evolving towards smaller steady state dimensions as insufficient tractions at the weak interface start influencing the development of plastic zone.

Falling R-curve-like behavior is also observed as the crack tip approaches a weakened interface zone covering the entire width of the specimen, eventually leading to unstable crack growth as the crack shot through the remainder of the weakened interface. Similar trends have been observed analytically and through experimental work around DCB specimens with heterogeneous interfaces [14,16,26]. As suggested earlier, the declining resistance results when the tractions integrated over the remaining ligament are insufficient to maintain the fracture resistance plateau seen in control specimens. When the crack advances far enough, the crack suddenly propagates along the weakened

interface in a rapid release of the available strain energy. This unstable crack growth could continue until tractions across the next control region begin building to arrest the crack. Dynamic effects associated with the unstable crack growth would also affect the distance over which a crack would grow in an unstable manner. Interestingly, the interactions of growing cracks with weakened interfaces could offer a means to study cohesive zones and traction-separation relationships from a new perspective, using techniques such as those developed by Gowrishankar et al. [27,28].

These observations indicate that the crack propagation behavior is influenced over a considerable distance both preceding and in the wake of weak interface regions that cover the entire width of the specimen. At this point, the distances mentioned above are tentative as the crack length is based solely on visual observations of crack tip location on the free surface. Based on thumbnail shapes observed using a dye-penetrant ink during separate mode-I DCB tests on control (type A) specimens, distances from weakened zones at the onset of reverse R-curve could be about 2 mm shorter than visually observed edge cracks, upon which the figures are based. (This thumbnail shape is often attributed to plane strain vs plane stress and anticlastic bending of adherends.) The one-sided error bar shown (only on a single data point to avoid confusion) in Fig. 6 and subsequent figures represents this distance uncertainty. Essentially, the crack could be this much longer, thereby affecting the crack tip position register with respect to the weakened zones.

Specimens D, E and F did not have a continuous weak interface across the entire width of the specimen, but each had four patterns of discrete weak interfaces separated by control regions. Details of the size of the localized weak interfaces ( $s$ ) within patterns, separation distances within ( $d$ ), and between successive patterns are provided in Fig. 2. For reference, the smallest defects among specimens D, E and F were approximately 6.5 times the adhesive layer thickness, a relative measurement with a basis in shear lag concepts and used in the literature [29]. All four patterns in specimen D had identical dimensions. In specimen E, the separation distance ( $d$ ) between the local weak interfaces within a pattern was increased in successive patterns, while keeping the local weak interface size ( $s$ ) constant for all four patterns. Control regions with similar lengths separated all four patterns in specimens D and E. In specimen F, the size of the local weak interface ( $s$ ) in a pattern was increased for successive patterns, keeping a constant separation distance ( $d$ ) between squares for all four patterns within the specimen. In specimen F the distance between the successive patterns was not similar as in specimens D and E, but this distance was decreased in successive patterns.

Fig. 7 shows failure surfaces of specimens D, E and F when tested under mode-I conditions. It was observed that, similar to failure modes shown schematically in Fig. 2, copper deposited regions showed apparent interfacial failures at the copper/adherend interface, while regions without copper deposition showed cohesive failures within the adhesive layer. Specimen D had four patterns of weak interfaces. All patterns had identical dimensions ( $s$ ,  $d$ ) and the length of the control regions between successive patterns was similar.

Figs. 8–10 show mode-I test results for specimens D, E and F, where the patterned regions are highlighted as in Fig. 6, along with the 2 mm estimate of crack length uncertainty on a single data point. The

**Table 1**  
SENB and compression test results.

	Compressive modulus (GPa)	Compressive yield strength <sup>a</sup> (MPa)	Tensile yield strength <sup>b</sup> (MPa)	$K_{Ic}$ (MPa m <sup>0.5</sup> )	Plane stress plastic zone diameter <sup>c</sup> (mm)
Average	2.45	37.77	28.33	1.16	0.17
Standard deviation	0.32	0.63	0.47	0.15	0.13

<sup>a</sup> Calculated using 1% offset.

<sup>b</sup> Equal to 75% of the yield strength in compression [25].

<sup>c</sup> Calculated using Eq. (4).

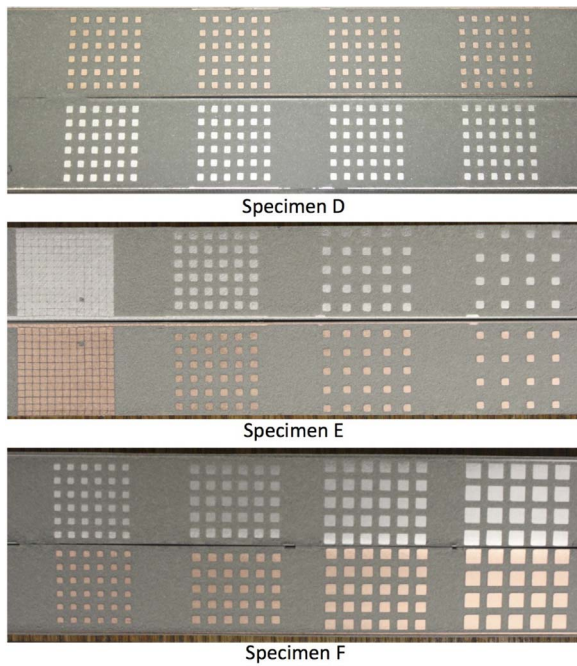


Fig. 7. Failure surfaces of specimens D, E and F tested in mode-I conditions. For reference, the smallest defects are approximately 6.5 times the adhesive layer thickness.

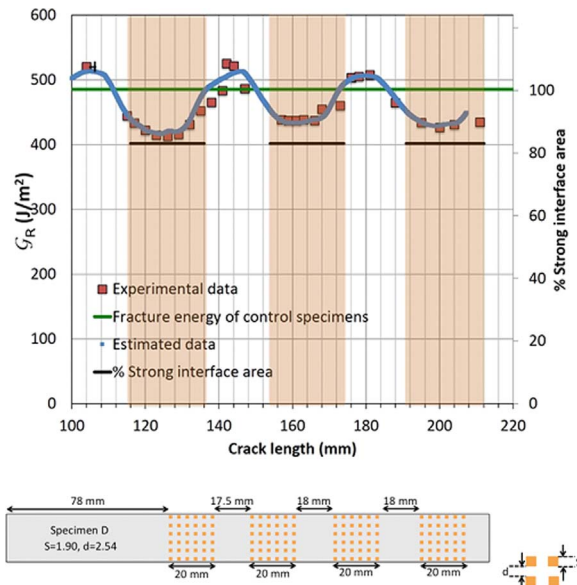


Fig. 8. Mode-I DCB test results and schematic representation of the weak interface pattern regions (shaded columns) for specimen D.

undulating fracture resistance arises as the growing crack grows through successive patterned and control regions with different areal fractions of copper present. Specimens D, E and F also suggested reversed R-curve behavior, albeit less in magnitude than that for specimen C, as the crack tip approached a patterned region, where fracture energy starts to decrease before the crack tip reaches a patterned region, falling to what appears to be plateaus within each given patterned region. An R-curve type of behavior is observed as the crack tip leaves the patterned region and enters the control regions between successive weak interfaces. The R-curve trend continues in the control region till the fracture energy reaches a maximum. For specimens D and E, the maximum fracture energy observed in successive control regions between patterns was reasonably constant and was similar to the fracture energy of specimens of type A. In specimen F, the maximum fracture

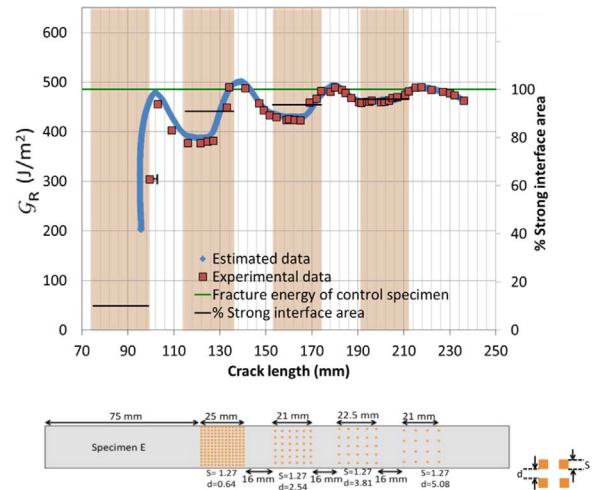


Fig. 9. Mode-I test results and schematic representation of the weak interface pattern regions (shaded columns) for specimen E.

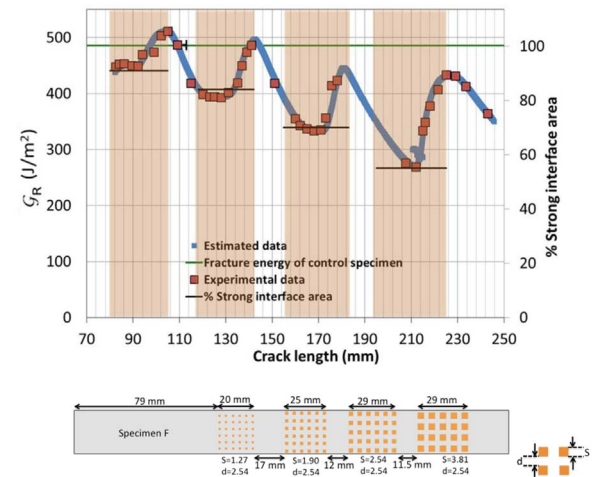


Fig. 10. Mode-I test results and schematic representation of the weak interface pattern regions (shaded columns) for specimen F.

energy observed in successive control regions between patterns (strong interface regions) decreases with smaller lengths of the control regions, indicating that in such cases, control regions were too short to permit full development of the R-curve. Also, it was observed that the minimum or the plateau fracture energy generally correlated with the fraction of good interface area within a pattern, as also shown in the figures by noting how the data points approach the solid horizontal lines showing percent of strong interface area on the right vertical axis, where 100% was normalized to the measured fracture energy of control specimens. In specimens D, E and F an appearance of a minimum or a plateau in the patterned regions having a range of *s* and *d* values hints towards the overall reduction in the fracture energy as the net weakened area increases rather than local contributions that arise due to micro-mechanisms at the crack tip, as will be discussed in a following section. Also of note is the fact that crack propagation remained stable in these specimens, perhaps because the continuous control regions among the weakened patterns retained sufficient traction capabilities.

In specimen C and for the first pattern in specimen E, a falling R-curve-like behavior is also observed as the crack tip approaches a weakened interface zone, eventually leading to unstable crack growth as the crack shot through the remainder of the weakened interface. This unstable crack growth could continue until tractions across the next control region begin building up and arrest the crack. In order to test this hypothesis, specimen G was prepared such that no long control

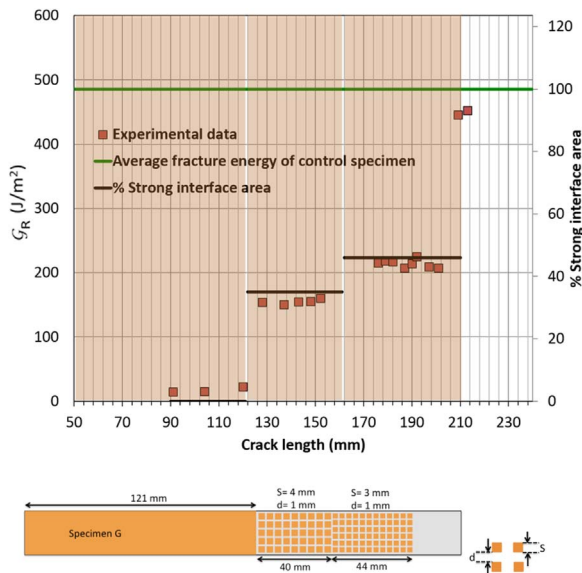


Fig. 11. Mode-I DCB test results and schematic representation of the weak interface pattern regions (shaded columns) for specimen G.

regions separated the patterned regions. Pattern dimensions ( $d, s$ ) were chosen such that the fraction of weak interface area decreased as the growing crack entered successive patterns, as shown schematically in Fig. 2. In specimen G the entire bonded area between the drilled holes up to the first pattern was coated with copper (100% coverage). Two patterns followed this fully coated area where separation between patterns was essentially the local weak interface separation distance ( $d$ ) for the next pattern. Mode-I test results for specimen G are shown in Fig. 11. In the test region where the entire bonded area was covered with copper, the fracture energies were similar to that of specimen B. In patterns following this region, it was observed that the fracture energy remained essentially constant within a given pattern and that the fracture energy increased with decreasing fraction of weak interfaces.

Specimens D, E, F and G patterns contained several discrete localized weak interfaces along the length of the specimens. Along the width and the length of the specimens, the localized weak interfaces within a pattern were separated by good (control) interfaces. In specimen H, the localized weak interfaces were separated along the width of the specimens but they were continuous along the length of the specimens, as shown in Fig. 2. This particular specimen type is similar to that used by Budzik et al. while studying the effect of weak interfaces on the fracture energy of an adhesive joint where a continuous weak interface was created throughout the length of the specimen [30]. As discussed for Fig. 3, copper deposited regions showed an apparent interfacial failure at copper/adherend interface, while regions without copper depositions showed cohesive failures within the adhesive layer. Mode-I test results for specimen H are shown in Fig. 12, revealing similar R-curve type trends as observed for specimens D, E, F and G. Also the maximum in the fracture energy within control regions correlated with the size of the control regions between successive patterns indicating that control regions were too short to result in fully developed R-curves.

The figures above have suggested a correlation between the measured fracture energies and the fraction of non-weakened bond area. Fig. 13 compiles this information, showing the minimum fracture energy values within patterned regions of specimens D, E, F, G, H and fracture energies of control specimens of type A and B plotted against the area fraction of good interfaces within the pattern. Also, in specimens D, E, F, G and H, the lengths of patterns were more than twice the distance between a pattern region and the onset of reverse R-curve type trends prior to a patterned region. Interestingly, it was observed that the measured fracture energy at the minimum within patterned weak

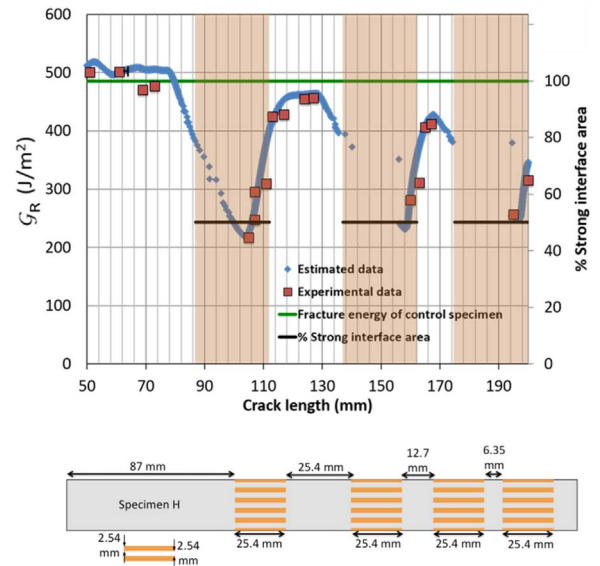


Fig. 12. Mode-I test results and schematic representation of the weak interface pattern regions (shaded columns) for specimen H.

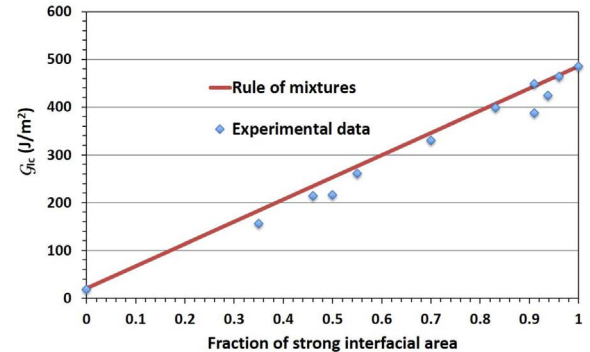


Fig. 13. The minimum fracture energy within a patterned region as a function of the area fraction of weak interface regions and the rule of mixtures according to Eq. (5).

interfaces of various densities with several sizes and separations were accurately modeled by a rule of mixtures, which is also plotted in Fig. 13:

$$G_{Total} = A_{Weak} G_{Weak} + A_{Strong} G_{Strong} \tag{5}$$

where  $G_{Total}$  is an effective fracture energy,  $G_{Weak}$  is an interfacial fracture energy at the Cu/Al interface from Fig. 4,  $G_{Strong}$  is the cohesive fracture energy of the adhesive for the geometry used in this study,  $A_{Weak}$  and  $A_{Strong}$  are, respectively, the area fractions of the weak and the strong interfaces within an entire patterned region determined using mask pattern dimensions.

It is interesting to note that Fig. 13 includes data from all the patterns used in this study. As shown in Fig. 2, these patterns contained localized weak interfaces of several sizes and several separation distances. The rule of mixtures agreement is, after all, consistent with the energy per unit area required to propagate a crack that is the basis of fracture mechanics. The agreement with the rule of mixtures is in contrast to results observed by Chan et al. for adhesive joints containing patterns of weak interfaces and bonded with a soft adhesive [31], during which higher or lower fracture energies than those predicted by the rule of mixtures were observed, depending upon the shape of weak or strong discrete interfaces facing the crack tip. Chung and Chaudhury et al. [32] studied the behavior of adhesion and crack propagation in patterned adhesive films. The adhesive films consisted of silicone elastomer patterned using longitudinal, lateral and crosswise incisions. Significant enhancement in fracture energy was observed for crosswise

incisions, which was attributed to crack pinning mechanisms at the incisions. However, it must be noted that the modulus of structural epoxy adhesive used in the current study is several orders of magnitude higher than the typical modulus range of a soft adhesive. In this study, mode-I results even with very small defects approximately 6.5 times the adhesive layer thickness of 0.2 mm, showed that the growing crack found most of the defects. Based on numerical studies using a cohesive zone model (CZM), Guan et al. have shown that detection of weak interface by a growing crack is a function of peak interfacial tractions available at the interface [28].

### 3.2. Mixed mode test results

The locus of failure in an adhesive joint and the resulting fracture energy are often reported to depend on the applied mode mixity [1,3]. Under mixed mode conditions, the stress state ahead of a crack tip often tends to drive the growing crack toward the adherend whose bonded surface is in tension. Thus, by using mixed mode loading, cracks can often be steered preferentially towards one adherend or the other. As shown earlier in Fig. 8, when the specimen D was tested in mode-I conditions, R-curve type trends were observed around patterned regions. Also the onset of reverse R-curve trends was observed when the observed crack tip was within 8 to 10 mm of the patterned regions. Fig. 14 shows failure surfaces around patterned region of type D specimen when tested in mixed mode conditions such that the adherend surface with weak interfaces was in axial tension due to bending. This leads to a stress state ahead of the crack tip that steers the crack towards the adherend containing the weak interface patterns (globally  $\psi = +60^\circ$  with reference to the weakened interface).

From Fig. 14, it is observed that, unlike the failure modes observed for mode-I conditions, 8% weak interface regions within a pattern were not detected by the propagating crack. Interestingly, the growing crack debonds fewer of the weakened areas when the crack is steered towards the weakened interface than seen under mode-I loading. Also, many local weak interfaces were only partially detected, with a cohesive

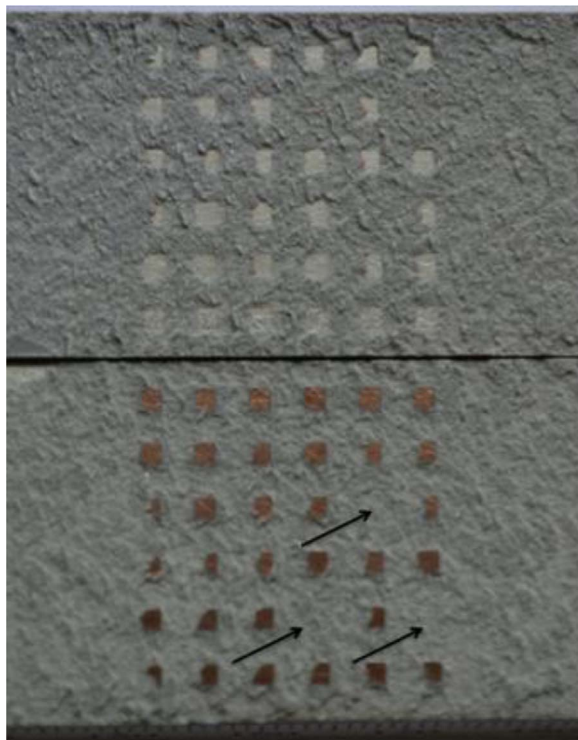


Fig. 14. Failure surfaces of specimen D when tested in mixed mode ( $\psi = +60^\circ$ ) conditions, where arrows point to undetected weak interface areas.

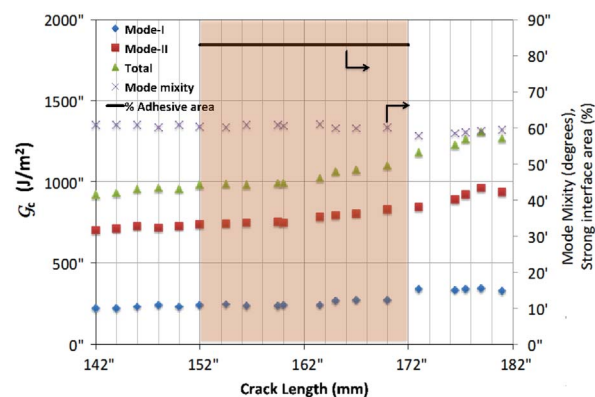


Fig. 15. Mixed mode ( $\psi = +60^\circ$ ) test results for specimen D with right side Y-axis representing mode mixity (degrees) and fraction of strong interface area (%).

failure in the adhesive layer over a portion of these weak interface regions. This is likely associated with the more complex hackle failure mode experienced when mode-II loading is present. DCB test results for specimen D when loaded under mixed mode conditions for a crack tip approaching and passing through a patterned area are shown in Fig. 15.

Interestingly, when a type D specimen was tested under mixed mode conditions, no R-curve type trends were observed either preceding or in the wake of patterned regions. Mode-I test data around the identical patterns is shown in Fig. 8. As shown in Fig. 10 under mode-I conditions fracture energy remained reasonably constant as the crack tip approached and entered an identical patterned region. Thus the same weak interface pattern when tested in mixed mode conditions did not show a significant effect on the fracture energy compared to the approximately 20% drop in the fracture energy in the patterned region when loaded in mode-I. Interfacial fracture toughness is known to be strongly dependent upon the mode mixity angle [33–35]. In light of such reports, higher interfacial resistance often associated with shear loading might provide sufficient interfacial tractions needed for the plasticity ahead of the crack to remain fully developed, leading to an absence of R-curve type trends in mixed mode conditions, at least for this specimen configuration.

Fig. 16 shows failure surfaces of identically patterned DCB specimens tested in mode-I and under mixed mode conditions (globally  $\psi = -60^\circ$ ) such that adherend bending put the weakened surface in axial compression, resulting in a stress state ahead of the crack tip which should drive the crack away from the weak interfaces.

It was observed that almost all the weak interfaces in patterns were detected by the crack tip in mode-I conditions, while in mixed mode conditions ( $\psi = -60^\circ$ ) very few local weak interfaces were detected by the growing crack, resulting in predominantly cohesive failures within the adhesive layer, even in the presence of very weak local interfaces in the patterned regions, confirming the possibility of diverting failures away from small but very weak interfaces. The observations reported in this study under mixed mode loading conditions are similar to that reported by Guan et al. whose numerical studies indicated that remote mixed mode loading is capable of either steering the crack into the weakened area, or away from it [28]. Their results also showed that defect size and interfacial peak traction were important in determining the crack path trajectory in linearly elastic materials.

It should be noted that the above results are based on a single set of pattern dimensions ( $s, d$ ) and for the geometry and materials used in this study. Nevertheless, these are interesting outcomes when considered in terms of potential applications such as controlled disassembly of the adhesive joints. For example, although based on preliminary and limited results, patterned bonds suggest possibilities to tune the mode-I fracture energy without significantly affecting mixed mode fracture behavior. Though it should be noted that under actual service applications, factors such as environmental conditions, fatigue

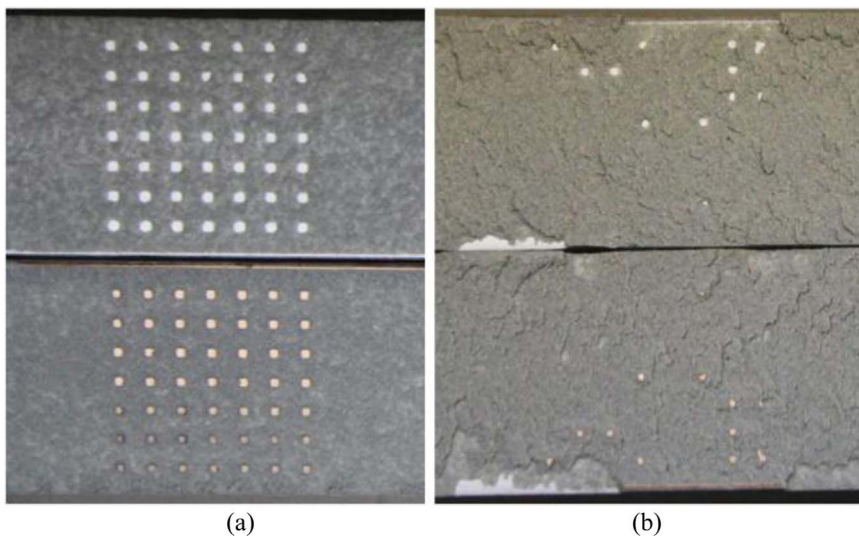


**Fig. 16.** Failure surfaces of identically patterned DCB specimens tested under (a) mode-I ( $\psi = 0^\circ$ ) and (b) mixed mode loading conditions ( $\psi = -60^\circ$ ) with defect size approximately 1.5 times the adhesive bondline thickness.

loading, or other factors could affect trends observed in this study.

#### 4. Conclusions

A technique is reported for creating well-defined and quantifiable localized weak interfaces on base-acid treated aluminum adherends using physical vapor deposition of copper. By using this technique to create several systematic patterns, the effect of the presence of localized interface defects on the performance of structural epoxy adhesive bonds was studied. Under mode-I loading conditions, the presence of localized weak interfaces influenced the fracture energy of a propagating debond over a considerable distance both before and following a local pattern of weakened interfaces. A reverse R-curve behavior was observed for a crack tip approaching a localized weak interface while rising R-curve type behavior was observed for a crack re-entering a control region. Furthermore, the mode-I fracture energy scaled with the area fraction of weak interfaces, according to the rule of mixtures. For the adhesive system and joint geometry used in this study, it was observed that under mixed mode loading such that the bonding surface with defects is in tension, the growing crack tip detects most of the defects but does not show a significant effect on the fracture energy. In contrast, a crack could be made to avoid exceptionally weak interfaces when loaded under mixed mode conditions such that the bonding surface with defects is in axial compression. This possibility combined with an ability to tune fracture energies in mode-I conditions may offer joint design options to allow a joint to either tolerate or be more susceptible to interfacial defects, offering the ability to tailor joint performance, designed failure modes, or easier disassembly. Furthermore, the reverse R-curve behavior seen as a propagating crack approaches a weakened material or interface region opens a potential opportunity for further elucidating cohesive zone tractions in material systems.

#### Acknowledgements

The authors gratefully acknowledge the financial support of the National Science Foundation through NSF/CMMI Award No. 0826143, as well as their support under DMR-0415840 for the construction of the dual actuator load frame used in this research. We would also like to thank the LORD Corporation (Cary, NC) for supplying adhesives needed for this work. In addition, we acknowledge use of facilities in the Biomedical Engineering and Mechanics and Chemistry Departments, as well as the Macromolecules and Interfaces Institute for fostering interdisciplinary research in adhesion science.

#### References

- [1] Fleck NA, Hutchinson JW, Suo ZG. Crack path selection in a brittle adhesive layer. *Int J Solids Struct* 1991;27:1683.
- [2] Daghyani HR, Ye L, Mai YW. Effect of thermal residual stress on the crack path in adhesively bonded joints. *J Mater Sci* 1996;31:2523.
- [3] Chen B, Dillard DA. The effect of the T-stress on crack path selection in adhesively bonded joints. *Int J Adhes Adhes* 2001;21:357.
- [4] Parvatareddy H, Dillard DA. Effect of mode-mixity on the fracture toughness of Ti-6Al-4V/FM-5 adhesive joints. *Int J Fract* 1999;96:215.
- [5] Liechti KM, Liang YM. Influence of specimen geometry on interfacial fracture resistance measurements. In: Winter annual meeting of the American Society of Mechanical Engineers. Publ by ASME; 1991.
- [6] Chen B, Dillard DA, Dillard JG, Clark Jr RL. Crack path selection in adhesively bonded joints: the roles of external loads and specimen geometry. *Int J Fract* 2002;114:167.
- [7] Dillard DA, Singh HK, Pohlit DJ, Starbuck JM. Observations of decreased fracture toughness for mixed mode fracture testing of adhesively bonded joints. *J Adhes Sci Technol* 2009;23:1515.
- [8] Chen B, Dillard DA, Dillard JG, Clark RL. Crack path selection in adhesively-bonded joints: the role of material properties. *J Adhes* 2001;75:405.
- [9] Xia SM, Ponsen L, Ravichandran G, Bhattacharya K. Adhesion of heterogeneous thin films 2: adhesive heterogeneity. *J Mech Phys Solids* 2015;83:88.
- [10] Van der Sluis O, Remmers JJC, Thurlings MAC, Welling BJ, Noijen SPM. The competition between adhesive and cohesive fracture at a micro-patterned polymer-metal interface. *Key Eng Mater* 2014;577–578:225.
- [11] Ramrus DA, Berg JC. Enhancement of adhesion to heterogeneously patterned substrates. *Colloids Surf A: Physicochem Eng Asp* 2006;273:84.
- [12] Budzik MK, Jumel J, Shanahan MER. Antagonist adhesion effects due to variable substrate surface. *Soft Matter* 2012;8:8321.
- [13] Chopin J, Prevost A, Boudaoud A, Adda-Bedia M. Crack front dynamics across a single heterogeneity. *Phys Rev Lett* 2011;107:144301.
- [14] Cuminatto C, Parry G, Braccini M. A model for patterned interfaces debonding – application to adhesion tests. *Int J Solids Struct* 2015;75:122.
- [15] Dalmas D, Barthel E, Vandembroucq D. Crack front pinning by design in planar heterogeneous interfaces. *J Mech Phys Solids* 2009;57:446.
- [16] Tvergaard V, Hutchinson JW. Analyses of crack growth along interface of patterned wafer-level Cu–Cu bonds. *Int J Solids Struct* 2009;46:3433.
- [17] Reedy ED. Effect of patterned nanoscale interfacial roughness on interfacial toughness: a finite element analysis. *J Mater Res* 2008;23:3056.
- [18] Heslehurst RB. Observations in the structural response of adhesive bondline defects. *Int J Adhes Adhes* 1999;19:133.
- [19] Nicoli E, Dillard DA, Frazier CE, Zink-Sharp A. Characterization of mixed-mode I/II fracture properties of adhesively bonded yellow-poplar by a dual actuator test frame instrument; 2012.
- [20] Kinloch AJ, Shaw SJ. The fracture resistance of a toughened epoxy adhesive. *J Adhes* 1981;12:59.
- [21] Ameli A, Papini M, Schroeder JA, Spelt JK. Fracture R-curve characterization of toughened epoxy adhesives. *Eng Fract Mech* 2010;77:521.
- [22] Arias M, Frontini P, Williams R. Analysis of the damage zone around the crack tip for two rubber-modified epoxy matrices exhibiting different toughenability. *Polymer* 2003;44:1537.
- [23] Papini M, Fernlund G, Spelt JK. Effect of crack-growth mechanism on the prediction of fracture load of adhesive joints. *Compos Sci Technol* 1994;52:561.
- [24] Hunston DL, Kinloch AJ, Wang SS. Micromechanics of fracture in structural adhesive bonds. *J Adhes* 1989;28:103.
- [25] Kinloch AJ. Adhesion and adhesives: science and Technology. London; New York: Chapman and Hall; 1987.

- [26] Kendall K. Control of cracks by interfaces in composites. *Proc R Soc Lond Ser A, Math Phys Sci* 1975;341:409.
- [27] Gowrishankar S, Mei HX, Liechti KM, Huang R. A comparison of direct and iterative methods for determining traction-separation relations. *Int J Fract* 2012;177:109.
- [28] Guan YL, Ohanehi DC, Batra RC, Dillard DA. Using cohesive zones to model adhesive bond fracture in the presence of locally weakened interfaces. *Int J Adhes Adhes* (In review).
- [29] Chen B, Dillard DA. Numerical analysis of directionally unstable crack propagation in adhesively bonded joints. *Int J Solids Struct* 2001;38:6907.
- [30] Budzik MK, Jumel J, Shanahan MER. Adhesive fracture of heterogeneous interfaces. *Philos Mag* 2013;93:2413.
- [31] Chan EP, Ahn D, Crosby AJ. Adhesion of patterned reactive interfaces. *J Adhes* 2007;83:473.
- [32] Chung JY, Chaudhury MK. Roles of discontinuities in bio-inspired adhesive pads. *J R Soc Interface* 2005;2:55.
- [33] Tvergaard V, Hutchinson JW. The influence of plasticity on mixed mode interface toughness. *J Mech Phys Solids* 1993;41:1119.
- [34] Liechti KM, Chai YS. Asymmetric shielding in interfacial fracture under inplane shear. *J Appl Mech-Trans ASME* 1992;59:295.
- [35] Liechti KM, Chai YS. Biaxial loading experiments for determining interfacial fracture-toughness. *J Appl Mech-Trans ASME* 1991;58:680.